Journal of Sound and Vibration 329 (2010) 5434–5451

Contents lists available at ScienceDirect

Journal of Sound and Vibration

journal homepage: www.elsevier.com/locate/jsvi

Delay-induced dynamics of an axially moving string with direct time-delayed velocity feedback

L.F. Lü [a,b], Y.F. Wang [a,b,*], X.R. Liu [a,b], Y.X. Liu [a,b]

[a] Department of Engineering Mechanics, Dalian University of Technology, 2 Linggong Road, Dalian 116024, China
[b] State Key Laboratory of Structural Analysis for Industrial Equipment, Dalian 116024, China

ARTICLE INFO

Article history:
Received 8 October 2009
Received in revised form
30 March 2010
Accepted 28 June 2010
Handling Editor: L.N. Virgin
Available online 5 August 2010

ABSTRACT

The local dynamics of an axially moving string under aerodynamic forces is investigated with a time-delayed velocity feedback controller. The retarded differential difference governing equation is obtained in modal coordinates of a two-degree-of-freedom system through Galerkin's discretization procedure. The stability of trivial equilibrium is examined with the change of counting multiplicity of eigenvalue with positive real part. The Hopf bifurcation curves are determined in the controlling parameter spaces. With the aid of the center manifold reduction, a functional analysis is carried out to reduce the modal equation to a single ordinary differential equation of one complex variable on the center manifold. The approximate analytical solutions in the vicinity of Hopf bifurcations are derived in the case of primary resonance. The curves of excitation–response and frequency–response curves are shown with the effect of time delay. The stability analysis for steady-state periodic solutions of the reduced system indicates the onset of local control parameter for vibration control and response suppression. Moreover, the Poincaré–Bendixson theorem and energy considerations are used to investigate the existences and characteristics of quasi-periodic solutions when stability of the periodic solution is lost. Numerical results demonstrate the validity of the analytical prediction. Two different kinds of quasi-periodic solutions are found.

1. Introduction

Machinery belts, textile fibers, aerial cable tramways, power transmission chains and high-speed magnetic tapes are important mass and energy transfer systems in engineering practice. Analysis of transverse vibration response plays an important role in industrial design of these axially moving continua. From the mechanical point of view, axially moving strings are flexible and easily undergo large deformation. The transverse oscillations can be generated due to the oscillations of elastic supports and other external excitations. Consequently, the life expectancy and operation reliability of the strings can be degraded. It is noted that axially moving strings belong to gyroscopic systems with infinite numbers of degrees-of-freedoms loaded by Coriolis force resulted from flowing relative references. Mathematically, the motion of the string is governed by a second-order partial differential equation. The partial derivative with respect to both temporal and spatial variables known as the term of the convective acceleration renders complex, speed-dependent modes, which brings great challenge in finding closed-form solutions for nonlinear systems. Previous investigations have concentrated on the

* Corresponding author at: Department of Engineering Mechanics, Dalian University of Technology, Dalian 116024, China. Tel.: +86 411 84706561x8050; fax: +86 411 84706571.
E-mail address: yfwang@dlut.edu.cn (Y.F. Wang).

0022-460X/$ - see front matter © 2010 Elsevier Ltd. All rights reserved.
doi:10.1016/j.jsv.2010.06.024

linear and nonlinear vibration responses of axially moving strings under various excitations and significant developments have been made for several decades (see e.g. [1–4]).

In recent years, there has been an increasing interest in suppressing the vibration of axially moving strings, since the controllability and observability conditions of distributed gyroscopic systems with point sensors and point actuators were presented [5,6]. It is found in [6] that only one collocated point sensor and actuator is required for vibration control of an axially moving string in both finite and infinite dimensional models. Vibration suppression of moving strings has been conducted using various techniques, e.g. the Laplace transform domain approach [7–9], wave cancellation method [10–12], the Lyapunov energy method [13,14] and the sliding mode technique [15,16]. The latter two methods are capable of controlling the vibration of axially moving strings with nonlinear models. However, they can only be implemented as boundary control, which is difficult to apply in some engineering circumstances [3]. Besides, the effect of external excitations has been neglected in most cases. It seems that these approaches are not well-suited to admit nonlinear dynamical characteristics, which are prevalent in transverse vibration of axially moving continua especially with high transport speed.

Time-delayed feedback is considered to be an ideal choice to suppress the nonlinear responses of dynamical systems, and time-delayed controllers have been applied to plenty of linear and nonlinear dynamical systems. A number of investigations [17–27] on simple nonlinear time-delayed models indicated that time delay can be regulated as a switch to stabilize the equilibrium and suppress the steady-state periodic solution. The concept of time delay has been adopted in the vibration control of axially moving strings. In [7] the design of stabilizing controller with time delay was carried out for both collocation and non-collocation of the sensors and actuators. The destabilizing effect of non-collocated sensors and actuators was eliminated for a translating string through introduction of a specific time delay in the feedback controller [8]. The non-collocated control with time delay was further extended to viscously damped strings [9]. Experimental verification of the time delay theory of a translating string was reported in [28]. Nevertheless, all of the previous controllers with time delay were designed based on the linear models of axially moving strings. No publications have been found addressing the dynamics of nonlinear models of axially moving strings with time-delayed feedback controller to the authors' knowledge. It is expected that the time-delayed feedback technique can be extended to vibration control of nonlinear axially moving strings. More specifically, the parameter of time delay can be adopted as an active parameter to stabilize the static configuration and to suppress the nonlinear vibrations of the string.

To better suppress undesirable motions of axially moving strings, it is important to solve the delay-induced vibration responses and understand its complex behavior related to the time delay. In the present paper, the delay-induced dynamics of an axially moving string under steady wind excitation is investigated. A linear, directly-delayed velocity-feedback controller pertaining to preserving the equilibrium of the original system is introduced. Geometrical nonlinearity caused by large deformation and velocity nonlinearity caused by aerodynamic excitations are both considered. The paper is organized as follows: The dynamical model of an axially moving string with time-delayed feedback control is provided in Section 2. A truncated, second-order system in modal coordinates is derived by Galerkin's discretization procedure. The explicit determination of the stability domain of the trivial equilibrium, in addition to curves of the Hopf bifurcation and critical time delay, is presented in Section 3 by evaluating counting multiplicities of the eigenvalues with positive real parts. In Section 4, the center manifold reduction in the vicinity of single Hopf bifurcation point as well as the homological equation for the local coordinate system on the center manifold is presented. The approximate analytical periodic solutions and their stabilities for both the self-excited system and primary resonance system are obtained in Section 5. The existence of two different kinds of quasi-periodic solutions is also discussed with the aid of the Poincaré–Bendixson theorem and an energy-like function. Illustrative examples are presented in Section 6, where the analytical and numerical results are compared. The local control parameters for suppressing the steady-state responses are shown. Finally, discussions and conclusions are given in Section 7.

2. Problem statement and formulation

A sagged string that axially moves with a constant speed between two fixed eyelets is depicted in Fig. 1. The string is subjected to one pair of collocated sensor and actuator for control of transverse displacement response denoted by $w(x,t)$.

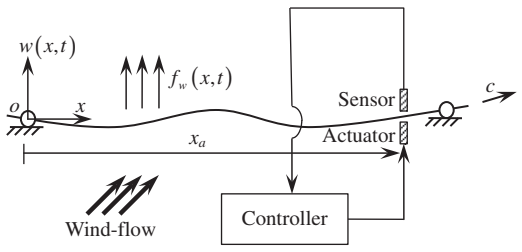

Fig. 1. A sketch of an axially moving string with a collocated time-delayed velocity feedback controller under wind excitation.

Following the non-dimensionalization of [29] and considering large deformation of the string, the governing equation of the closed-loop system can be derived as

$$\ddot{w}(x,t)+2c\dot{w}'(x,t)+(c^2-c_0^2)w''(x,t)+\delta(\dot{w}(x,t)+cw'(x,t))-\frac{3}{2}k_3w'^2(x,t)w''(x,t)$$
$$=f_w(x,t)+f_e(x,t)+u(x_a,\tau)\qquad(0\le x\le 1). \tag{1}$$

where primes and dots denote partial derivatives with respect to x and t, respectively; c is the non-dimensional transport speed; c_0 is the non-dimensional axial tensile force; δ is the viscous damping coefficient related to the absolute velocity of the moving string; k_3 is the non-dimensional extensional rigidity of the string. The three terms of the right-hand side of Eq. (1) represent the aerodynamic "lift" force, the distributed external excitation and the active control force on the string, respectively. In addition, the boundary condition of displacement is $w(0,t)=w(1,t)=0$. Notice that the direction of wind flow is assumed perpendicular to the Oxw-plane.

The vertical component of non-dimensional aerodynamic forces can be expressed as $f_w(x,t)=f_1\dot{w}(x,t)+f_3\dot{w}^3(x,t)$ where $f_1=1/2\alpha_0c_1\nu$, $f_3=1/2\alpha_0c_3\nu^{-1}$, ν is the average velocity of the wind. c_1, c_3 and α_0 are aerodynamic coefficients depending on the cross section of the string, angle of attack and the flow conditions. For direct time-delayed velocity feedback with the collocated sensor and actuator, the sensor measures the velocity of string at the sensor location. Then, the signal is amplified by a gain and delayed with a delay-machine. This control input is re-applied to the string by an actuator. Therefore, the active control force can be given by $u(x_a,\tau)=\alpha\dot{w}(x,t-\tau)\boldsymbol{\delta}(x-x_a)$, where α is the velocity feedback gain, τ and x_a are time delay constant and location of the sensor and the actuator, respectively. They are also controlling parameters to be designed. $\delta(\cdot)$ is Dirac's delta function.

A second-order Galerkin's discretization scheme is adopted to expand the displacement: $w(x,t)=\sum q_i(t)\sin(i\pi x)$, $i=1,2$, which yields the nonlinear equations in the truncated modal coordinates:

$$\ddot{q}_1+\mu\dot{q}_1-a_1\dot{q}_2+kq_1-a_2q_2-3/4f_3(\dot{q}_1^3+2\dot{q}_1\dot{q}_2^2)+3k_3\pi^4(1/8q_1^3+q_1q_2^2)+\alpha_1\dot{q}_{1\tau}+\alpha_2\dot{q}_{2\tau}=0$$
$$\ddot{q}_2+a_1\dot{q}_1+\mu\dot{q}_2+a_2q_1+4kq_2-3/4f_3(\dot{q}_2^3+2\dot{q}_2\dot{q}_1^2)+3k_3\pi^4(2q_2^3+q_2q_1^2)+\alpha_2\dot{q}_{1\tau}+\alpha_3\dot{q}_{2\tau}=0, \tag{2}$$

where

$$\dot{q}_{1\tau}=\dot{q}_1(t-\tau),\quad \dot{q}_{2\tau}=\dot{q}_2(t-\tau),\quad k=\pi^2(c_0^2-c^2),\quad a_1=16c/3, a_2=8\delta c/3,$$
$$\mu=\delta-f_1,\quad \alpha_1=-2\alpha\sin^2(\pi x_a),\ \alpha_2=-2\alpha\sin(\pi x_a)\sin(2\pi x_a), \alpha_3=-2\alpha\sin^2(2\pi x_a).$$

It can be seen that if the sensor and the actuator are not placed at nodes of modes to be controlled, i.e. $\alpha_i\neq 0$, $i=1,2,3$, the feedback gain α and time delay τ can be used as active parameters to control the axially moving string, which is in agreement with the controllability and observability condition of distributed gyroscopic systems [6].

3. Stability of the equilibrium and Hopf bifurcation

To analyze the local stability of the system, the equilibrium is examined by removing the time-related terms in Eq. (2), yielding

$$kq_1-a_2q_2+3k_3\pi^4(1/8q_1^3+q_1q_2^2)=0,$$
$$a_2q_1+4kq_2+3k_3\pi^4(2q_2^3+q_2q_1^2)=0, \tag{3}$$

which further gives

$$kq_1^2+4kq_2^2+3k_3\pi^4(1/8q_1^4+2q_1^2q_2^2+2q_2^4)=0. \tag{4}$$

Eq. (2) has a unique equilibrium point when the transport speed is less than the critical transport speed (i.e. $c<c_0$): $(q_1,\dot{q}_1,q_2,\dot{q}_2)=(0,0,0,0)$which represents the static configuration of the string. There may exist non-trivial equilibrium points when the string travels with supercritical speeds. Although the current concern is limited to subcritical transport speed, the non-trivial equilibrium points of supercritical moving system can be studied similarly after coordinate transformation. The characteristic equation corresponding to the linear equation of Eq. (2) evaluated at the trivial equilibrium point is

$$P(\lambda)=\lambda^4+\lambda^3(b_3+d_3e^{-\tau\lambda})+\lambda^2(b_2+d_2e^{-\tau\lambda})+\lambda(b_1+d_1e^{-\tau\lambda})+b_0 \tag{5}$$

where λ is the eigenvalue of the system in Eq. (2), and

$$b_0=a_2^2+4k^2,\quad b_1=5\mu k+2a_1a_2,\quad b_2=a_1^2+\mu^2+5k,$$
$$b_3=2\mu,\quad d_1=4k\alpha_1+k\alpha_3,\quad d_2=(\alpha_1+\alpha_3)\mu,\quad d_3=\alpha_1+\alpha_3. \tag{6}$$

For the uncontrolled system, the explicit conditions were provided by Wang et al. [30] and Lu et al. [31], both taking the transport speed and wind speed as control parameters, for loss of stability and generation of stable limit cycles via the Hopf bifurcation based on the Routh–Hurwitz stability criterion. It can be seen that the stability conditions of the uncontrolled system and the controlled system without time delay are essentially the same if the coefficients of the characteristic polynomial are detuned by $b_1+d_1\to\tilde{b}_1$, $b_2+d_2\to\tilde{b}_2$, $b_3+d_3\to\tilde{b}_3$. Therefore, the stability conditions of the controlled

system without time delay have the same form as in [31]:

$$\tilde{b}_0>0,\quad \tilde{b}_1>0,\quad \tilde{b}_2>0,\quad \tilde{b}_3>0,\quad \tilde{b}_1(\tilde{b}_3\tilde{b}_2-\tilde{b}_1)-\tilde{b}_3^2\tilde{b}_0>0 \tag{7}$$

and the Hopf bifurcation occurs when $\tilde{b}_1(\tilde{b}_3\tilde{b}_2-\tilde{b}_1)-\tilde{b}_3^2\tilde{b}_0=0$.

Basically, the stability condition for a controlled system with time delay is different from an uncontrolled system since the characteristic polynomial is an exponential-transcendental function that possesses up to infinite number of eigenvalues. Further, the stability domain of the controlled system may be variable in the parameter space when time delay changes. It has been learned that there are only a finite number of solutions that lies in the right half-complex plane for retarded differential difference equation if the characteristic equation is an entire function [32,33]. To determine the stability domain of the retarded differential difference equation, a Lemma for a polynomial–exponential characteristic system was presented in [34] to analyze the stability of equilibrium of a single-action mechanism using a scalar equation with a constant time delay. Xu and Yu [21] extended the method to a second-order characteristic equation of a self-sustained system with delayed velocity feedbacks. Their work is advanced in the present paper to a generalized theorem for any polynomial–exponential equations with constant time delays.

Theorem 1. *Consider a generalized polynomial–exponential characteristic function* $P(\lambda,\tau)=\sum_{i=0}^{m}\lambda^i(\hat{b}_i+\hat{d}_ie^{-\tau_i\lambda})$, *where* $\hat{b}_i,\ \hat{d}_i\in\mathbb{R},\ \hat{b}_i\neq 0$, *and* $\tau_i\geq 0, 0\leq i\leq m$. *Denote the number of roots of equation* $P(\lambda,\tau)=0$, *where* $\mathrm{Re}(\lambda)>0$, *as* $M(\tau)$ *the counting multiplicity. Then* $M(\tau)$ *can only be changed when* λ *passes through the imaginary axis as one of the time delays* τ_l *is varied.*

Proof. Let $\lambda=\lambda(\tau)$ be a root of equation $P(\lambda,\tau)=0$ that satisfies $0<\mathrm{Re}(\lambda)<\infty$. Since $P(\lambda,\tau)$ is a polynomial–exponential function, $\lambda(\tau)$ is an analytical function of τ. Based on Rouché's theorem (see e.g. [35]), there exists an $\varepsilon>0$ such that for $|\tau-\upsilon|<\varepsilon$, $\lambda(\upsilon)$ has the same multiplicity as $\lambda(\tau)$. Suppose that $M(\tau)$ changes without a single root appearing on the imaginary axis, then such a change can only occur when there is a root at infinity. Hence, there exists a $\tilde{\tau}$ and a sequence of $\{\tilde{\tau}^{(i)}\}$ such that $\lim_{i\to\infty}\tilde{\tau}^{(i)}=\tilde{\tau}$, $\lim_{i\to\infty}|\lambda(\tilde{\tau}^{(i)})|=\infty$, and $\mathrm{Re}(\lambda(\tilde{\tau}^{(i)}))\geq 0$, where $|\cdot|$ denotes complex modulus. As a result

$$\lim_{i\to\infty}|P(\lambda,\tau)/\lambda^m|=\lim_{i\to\infty}\left|\sum_{i=0}^{m}\lambda^{i-m}(\hat{b}_i+\hat{d}_ie^{-\tau_i\lambda})\right|=|b_m|\neq 0$$

which contradicts with $P(\lambda,\tau)=0$. □

For Eq. (5), it can be found that $m=4$, $b_4=1$ *and* $\tau_i=\tau$. Thus, Theorem 1 can be applied there by letting $\hat{b}_i\to b_i,\ \hat{d}_i\to d_i,\ i=0,1,2,3$, where b_i and d_i are expressed in Eq. (6). The above Theorem 1 implies that stability of equilibrium of system (2) can only be lost through the Hopf bifurcation since $\lambda\neq 0$ due to $b_0=a_2^2+4k^2>0$. Thus, the effect of time delay on stability of the equilibrium can be evaluated by examining the change of $M(\tau)$ using the eigen-polynomial in Eq. (5). Let $\lambda=I\beta$, where $I=\sqrt{-1}$ and $\beta>0$ is the bifurcation frequency of the equilibrium. Substituting λ in Eq. (5) and separating the real and imaginary parts yields

$$\begin{aligned}&\beta^4-\beta^2b_2+b_0=(\beta^3d_3-\beta d_1)\sin(\tau\beta)+\beta^2d_2\cos(\tau\beta),\\&-\beta^3b_3+\beta b_1=-\beta^2d_2\sin(\tau\beta)+(\beta^3d_3-\beta d_1)\cos(\tau\beta),\end{aligned} \tag{8}$$

which leads to the condition for the Hopf bifurcation

$$\beta_c^8+(b_3^2-d_3^2-2b_2)\beta_c^6+(2d_1d_3+b_2^2+2b_0-2b_1b_3-d_2^2)\beta_c^4+(b_1^2-2b_0b_2-d_1^2)\beta_c^2+b_0^2=0. \tag{9}$$

provided $(\beta_c^3d_3-\beta_cd_1)^2+\beta_c^4d_2^2\neq 0$ is satisfied. It is noticed from Eq. (9) that there are at most four critical frequencies depending on the parameters of system, which is different from a controlled system without time delay where there are no more than two critical frequencies. The bifurcation value of time delay τ_c can be obtained by solving Eq. (8):

$$\begin{aligned}&\tau_{cn,i}=\beta_{ci}^{-1}(s_i+2n\pi),\quad n=0,1,\ldots,\quad i=1,\ldots,4,\quad 0\leq s_i<2\pi,\\&\sin(s_i)=((\beta_{ci}^3d_3-\beta_{ci}d_1)^2+\beta_{ci}^4d_2^2)^{-1}((\beta_{ci}^4-\beta_{ci}^2b_2+b_0)(\beta_{ci}^3d_3-\beta_{ci}d_1)-\beta_{ci}^2d_2(\beta_{ci}b_1-\beta_{ci}^3b_3)),\\&\cos(s_i)=((\beta_{ci}^3d_3-\beta_{ci}d_1)^2+\beta_{ci}^4d_2^2)^{-1}((\beta_{ci}^3d_3-\beta_{ci}d_1)(\beta_{ci}b_1-\beta_{ci}^3b_3)+\beta_{ci}^2d_2(\beta_{ci}^4-\beta_{ci}^2b_2+b_0)).\end{aligned} \tag{10}$$

where β_{ci} and $\tau_{cn,i}$ represent the ith critical frequency and its nth time delay of bifurcation corresponding to β_{ci}, respectively.

The change of the counting multiplicity is identified by the sign $d\lambda/d\tau$ evaluated at the critical points. The transversality condition for the Hopf bifurcation can be satisfied if $d\lambda/d\tau\neq 0$. In the present study, the $d\tau/d\lambda$ is used for it is easily calculated by differentiating the characteristic equation (5):

$$\begin{aligned}\mathrm{Re}(d\tau/d\lambda)|_{\lambda=I\beta}=&((\beta^3d_3-\beta d_1)^2+\beta^4d_2^2)^{-1}(2\beta^2(2d_3d_1-d_2^2)-3\beta^4d_3^2-d_1^2)+((\beta^4-\beta^2b_2+b_0)^2+(\beta b_1-\beta^3b_3)^2)^{-1}\\&(4\beta^6+3\beta^4(b_3^2-2b_2)+2\beta^2(2b_0+b_2^2-2b_3b_1)-2b_2b_0+b_1^2)\end{aligned} \tag{11}$$

Hence,

$$\mathrm{sgn}(\mathrm{Re}(d\tau/d\lambda)|_{\lambda=I\beta})=\mathrm{sgn}(4\beta^6+3(b_3^2-d_3^2-2b_2)\beta^4+2(2d_1d_3+b_2^2+2b_0-2b_1b_3-d_2^2)\beta^2+(b_1^2-2b_0b_2-d_1^2)). \tag{12}$$

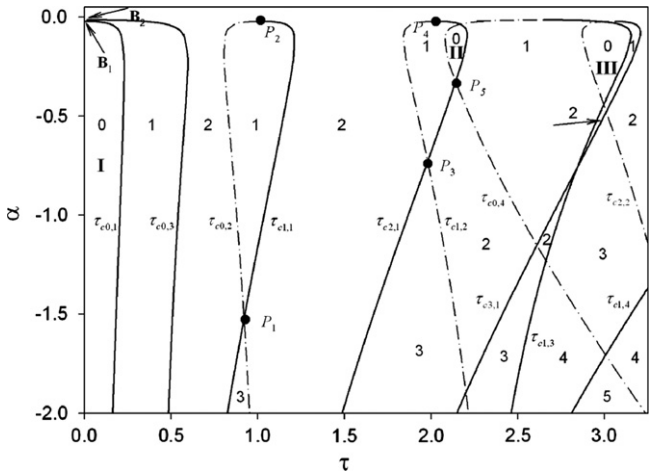

Fig. 2. Stability divisions in parameter spaces of feedback gain α and time delay τ. Integers 0–5 indicate the number of eigenvalues in the right half-plane of the complex space. **I**, **II**, and **III** denote the stability regions. The critical curves of time delay are computed by (10), denoted by $\tau_{cn,i}, n=0,1,2,\ldots, i=1,2,3,4$. The solid lines and the dash-dotted lines represent the increase or decrease of the counting multiplicity as time delay increases.

With the above-mentioned analysis, the stable domain in the parameter spaces can be identified as follows: First, obtain the bifurcation points and assess their stability at $\tau=0$ based on Eq. (6), and label the parameter spaces with 0, 1 or 2 as the value of $M(0)$. Second, solve the eigen-frequency equation (9) with the control parameter varying from the bifurcation point to obtain the critical time delay $\tau_{cn,i}$. Finally, check Eq. (12) for the transversality condition of Hopf bifurcation and update $M(\tau)$. The stable region of the equilibrium can be completely determined with the counting multiplicity being zero.

Consider a specific system as an illustrative example, where the parameters are chosen to be $c_0=1$, $c=0.5$, $\delta=0.04$, $\alpha_0=4.7766$, $c_1=0.2992$, $c_3=-0.2766$, $\nu=0.1$ and $x_a=\sqrt{2}/2$. The feedback gain α is considered as the governing parameter. In Fig. 2, the stability sub-domains and bifurcation curves of time delay in the parameter space of (α,τ) are shown, where solid and dash-dotted lines represent the critical curves cross which the counting multiplicity increases and decreases with an increasing time delay. For $\tau=0$, the frequencies and feedback gains of the first and second Hopf bifurcations are numerically obtained, shown as points $\mathbf{B}_1$ (6.1980, −0.02235)and $\mathbf{B}_2$ (2.3886, −0.01559), respectively. $\alpha<-0.02235$ is the only stable region for the controlled equilibrium configuration of the string without time delay. Multiple stable regions denoted by **I**, **II** and **III** are determined when the time delay is introduced. It is found in Fig. 2 that direct velocity feedbacks without time delay are robust for small lag of feedback since the adjacent region **I** is stable. Parameters in regions **II** and **III** with large time delay and small gain of velocity feedback can also be used to suppress vibration of the string. In addition, several non-resonant double Hopf bifurcation points are found in Fig. 2 where two different curves intersect with different directional derivatives at the bifurcation points (e.g. $\mathbf{P_1}$, $\mathbf{P_3}$, $\mathbf{P_5}$), two pairs of eigenvalues cross through the imaginary axis simultaneously. There exist rich dynamical behaviors near the non-resonant double Hopf point whose complete geometrical structures are still difficult to understand.

Next, results from numerical integrations using several time delays are given to show dynamics of the system (2) without external loadings. The integrations are carried out by the BS (2, 3) Runge–Kutta method [36] based on a standard Runge–Kutta formula and cubic Hermite interpolation among mesh points of time. Time histories and phase portraits of response for different time delays with $\alpha=0.2, \nu=0.1$ are shown in Fig. 3 using initial condition $(q_1,\dot{q}_1,q_2,\dot{q}_2)=(0.01,0,-0.05,0)$ at $t=0$ and trivial lag functions for $t<0$. It can be seen that vibration of the string is reduced by time delays for both small time delay of $\tau=0.1$(shown in Figs. 3(a) and 3(b)) and large time delay of $\tau=3$ (shown in Fig. 3(g) and (h)). A small time delay is advantageous since the transient response decays faster than that with a larger delay. Similar to uncontrolled systems [30,31], an isolated periodic solution, i.e. limit cycle, can be found in the phase plane after the equilibrium becomes unstable via the Hopf bifurcation, as shown in Fig. 3(c) and (d) with $\tau=0.5$ and (e) and (f) with $\tau=2.5$. The analytical solutions of the periodic solutions will be derived in the next section.

4. Center manifold reduction

The delayed variables are generally expanded into Taylor series in traditional perturbation schemes to investigate the delay-induced dynamics of nonlinear systems. More stringent results can be obtained by using the normal form theory and center manifold reduction [19,21,23,24,37]. The center manifold reduction theorem provides a systematic approach to reduce the infinitely dimensional state spaces of a delayed differential equation. The governing equation of axially moving

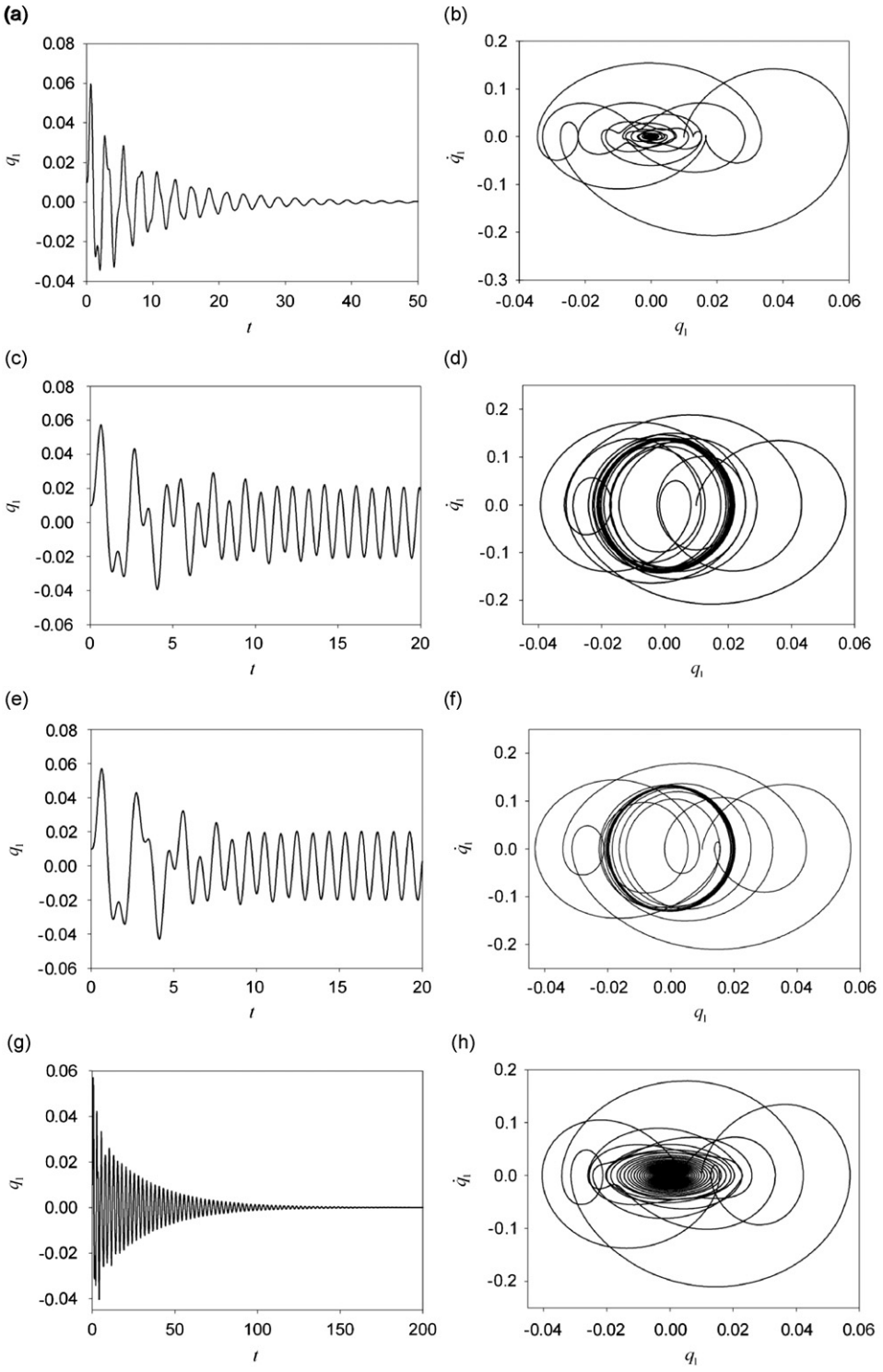

Fig. 3. Time trajectories and phase portraits for different time delays τ=0.1(a, b), τ=0.5(c, d), τ=2.5(e, f), and τ=3 (g, h) with velocity feedback gain α=0.2, ν=0.1.

strings with time delay is a functional differential equation and an infinite dimensional system in the mathematical sense. In the neighborhood of a single Hopf bifurcation point, the existence of a local integral manifold, which is homeomorphic to an open disk in a two-dimensional real space was studied in [38] and the properties of the manifold were established.

A functional analysis should be carried out in an abstract Banach space to reduce the infinite dimensional equation to a two dimensional one.

To investigate the effect of external excitation in the case of primary resonance, the string is assumed to be loaded by a distributed in-plane excitation: $f_a\cos(\overline{\Omega}_0 t)\sin(\pi x)$, where f_a and $\overline{\Omega}_0$ are non-dimensional forcing amplitude and frequency, respectively. To transform the differential difference equation (2) into a retarded functional differential equation, a Banach space $C([-\tau,0],R^4)$ of continuous functions is defined to map the interval $[-\tau,0]$ into R^4 with the norm $|\phi(\theta)|=\sup_{-\tau\le\theta<0}|\phi(\theta)|$ for any $\phi\in C$. The functional operator equation is obtained as

$$\dot{X}=LX_t+N_3(X_t(0))+\overline{F}_a \tag{13}$$

where

$$X=(x_1,x_2,x_3,x_4)^T\triangleq(q_1,\dot{q}_1,q_2,\dot{q}_2)^T,\quad X_t(\theta)=X(t+\theta),-\tau\le\theta\le 0.$$

The linear operator L, the forcing vector $\overline{F}_a$, and the nonlinear vector N_3 are defined as

$$\begin{gathered}LX_t=\int_{-\tau}^{0}[d\eta(\theta)]X_t(\theta),\\ \overline{F}_a=(0,\quad \bar{f}_a\cos(\overline{\Omega}_0 t),\quad 0,\quad 0)^T,\\ N_3(X_t(0))=\begin{pmatrix}0\\ 3/4f_3(x_{2t}^3(0)+2x_{2t}(0)x_{4t}^2(0))-3k_3\pi^4(1/8x_{1t}^3(0)+x_{1t}(0)x_{3t}^2(0))\\ 0\\ 3/4f_3(x_{4t}^3(0)+2x_{2t}^2(0)x_{4t}(0))-3k_3\pi^4(2x_{3t}^3(0)+x_{1t}^2(0)x_{3t}(0))\end{pmatrix},\end{gathered} \tag{14}$$

by using the Riesz representation theorem (see Hartig [39]) and the matrix-valued bounded variation

$$d\eta(\theta)=\begin{bmatrix}0 & \boldsymbol{\delta}(\theta) & 0 & 0\\ -k\boldsymbol{\delta}(\theta) & -\mu\boldsymbol{\delta}(\theta)-\alpha_1\boldsymbol{\delta}(\theta+\tau) & a_2\boldsymbol{\delta}(\theta) & a_1\boldsymbol{\delta}(\theta)-\alpha_2\boldsymbol{\delta}(\theta+\tau)\\ 0 & 0 & 0 & \delta(\theta)\\ -a_2\boldsymbol{\delta}(\theta) & -a_1\boldsymbol{\delta}(\theta)-\alpha_2\boldsymbol{\delta}(\theta+\tau) & -4k\boldsymbol{\delta}(\theta) & -\mu\boldsymbol{\delta}(\theta)-\alpha_3\boldsymbol{\delta}(\theta+\tau)\end{bmatrix}d\theta.$$

Taking wind speed v, velocity feedback gain α and time delay τ as the controlling parameters, it is assumed that Eq. (5) has two simple roots $\pm I\beta_c$ and the real parts of other roots are all negative at parameters v_c,α_c, and τ_c. Let $v=v_c+\overline{v}$, $\alpha=\alpha_c+\overline{\alpha}$, $\tau=\tau_c+\overline{\tau}$ and introduce a scaled time variable $t=\tau\bar{t}$, Eq. (13) can be transformed into

$$X'=L(0)X_t+L_1(\overline{v},\overline{\alpha},\overline{\tau})X_t+(\tau N_3(X_t(0))+P(X_t(0),\quad X_t(-1)))+\tau F_a \tag{15}$$

where

$$\begin{gathered}L(0)\phi(\theta)=\int_{-1}^{0}[d\eta_c(\theta)]\phi(\theta),\quad L_1(\overline{v},\overline{\alpha},\overline{\tau})\phi(\theta)=\int_{-1}^{0}[d\overline{\eta}(\theta,\overline{v},\overline{\alpha},\overline{\tau})]\phi(\theta),\\ P(X_t(0),\quad X_t(-1))=-\begin{pmatrix}0\\ \overline{\mu\tau}x_{2t}(0)+\overline{\alpha}_1\overline{\tau}x_{2t}(-1)+\overline{\alpha}_2\overline{\tau}x_{4t}(-1)\\ 0\\ \overline{\mu\tau}x_{4t}(0)+\overline{\alpha}_2\overline{\tau}x_{2t}(-1)+\overline{\alpha}_3\overline{\tau}x_{4t}(-1)\end{pmatrix},\end{gathered} \tag{16}$$

and

$$d\eta_c(\theta)=\begin{bmatrix}0 & \tau_c\boldsymbol{\delta}(\theta) & 0 & 0\\ -\tau_c k\boldsymbol{\delta}(\theta) & -\tau_c\mu_c\boldsymbol{\delta}(\theta)-\tau_c\alpha_{1c}\boldsymbol{\delta}(\theta+1) & \tau_c a_2\boldsymbol{\delta}(\theta) & \tau_c a_1\boldsymbol{\delta}(\theta)-\tau_c\alpha_{2c}\boldsymbol{\delta}(\theta+1)\\ 0 & 0 & 0 & \tau_c\delta(\theta)\\ -\tau_c a_2\boldsymbol{\delta}(\theta) & -\tau_c a_1\boldsymbol{\delta}(\theta)-\tau_c\alpha_{2c}\boldsymbol{\delta}(\theta+1) & -4\tau_c k\boldsymbol{\delta}(\theta) & -\tau_c\mu_c\boldsymbol{\delta}(\theta)-\tau_c\alpha_{3c}\boldsymbol{\delta}(\theta+1)\end{bmatrix}d\theta,$$

$$d\overline{\eta}(\theta,\overline{v},\overline{\alpha},\overline{\tau})=\begin{bmatrix}0 & \overline{\tau}\boldsymbol{\delta}(\theta) & 0 & 0\\ -\overline{\tau}k\boldsymbol{\delta}(\theta) & -\gamma_1\boldsymbol{\delta}(\theta)-\gamma_2\boldsymbol{\delta}(\theta+1) & \overline{\tau}a_2\boldsymbol{\delta}(\theta) & \overline{\tau}a_1\boldsymbol{\delta}(\theta)-\gamma_3\boldsymbol{\delta}(\theta+1)\\ 0 & 0 & 0 & \overline{\tau}\delta(\theta)\\ -\overline{\tau}a_2\boldsymbol{\delta}(\theta) & -\overline{\tau}a_1\boldsymbol{\delta}(\theta)-\gamma_3\boldsymbol{\delta}(\theta+1) & -4\overline{\tau}k\boldsymbol{\delta}(\theta) & -\gamma_1\boldsymbol{\delta}(\theta)-\gamma_4\boldsymbol{\delta}(\theta+1)\end{bmatrix}d\theta,$$

where

$$\begin{gathered}\mu_{1c}=\delta-1/2\alpha_0 c_1 v_c,\quad \overline{\mu}_1=-1/2\alpha_0 c_1\overline{v}\overline{\alpha}_1=-2\overline{\alpha}\sin^2(\pi x_a),\\ \alpha_{1c}=-2\alpha_c\sin^2(\pi x_a),\quad \alpha_{2c}=-2\alpha_c\sin(\pi x_a)\sin(2\pi x_a),\\ \overline{\alpha}_2=-2\overline{\alpha}\sin(\pi x_a)\sin(2\pi x_a),\quad \overline{\alpha}_3=-2\overline{\alpha}\sin^2(2\pi x_a),\quad \alpha_{3c}=-2\alpha_c\sin^2(2\pi x_a),\\ \gamma_1=(\mu_c\overline{\tau}+\tau_c\overline{\mu}),\quad \gamma_2=(\alpha_{1c}\overline{\tau}+\tau_c\overline{\alpha}_1),\quad \gamma_3=(\alpha_{2c}\overline{\tau}+\tau_c\overline{\alpha}_2),\quad \gamma_4=(\alpha_{3c}\overline{\tau}+\tau_c\overline{\alpha}_3).\end{gathered}$$

Defining the following operators for $\phi \in C([-1,0],\mathbf{R}^4)$:

$$D(0)\phi = \begin{cases} d\phi(\theta)/d\theta, & -1 \le \theta < 0 \\ L(0)\phi(\theta), & \theta = 0 \end{cases},$$

$$D_1(\theta,\overline{\nu},\overline{\alpha},\overline{\tau})\phi = \begin{cases} 0, & -1 \le \theta < 0 \\ L_1(\theta,\overline{\nu},\overline{\alpha},\overline{\tau})\phi(\theta), & \theta = 0 \end{cases},$$

$$R\phi = \begin{cases} 0, & -1 \le \theta < 0 \\ \tau N_3(X_t(0)) + P(X_t(0),X_t(-1)) + \tau F_a, & \theta = 0 \end{cases}. \tag{17}$$

Since $dX_t/d\theta = dX_t/dt$, Eq. (15) can be casted into the form

$$X'_t = D(0)X_t + D_1(\overline{\nu},\overline{\alpha},\overline{\tau})X_t + RX_t, \tag{18}$$

which involves a single unknown vector X_t rather than two vectors X and X_t as in Eq. (15).

The adjoint space $C^* = C([0,1],\mathbf{R}^4)$ should also be defined to decompose C. For any $\psi \in C^*$ the infinitesimal generator $D^*(0)$ of solution operator of the formal adjoint equation of (18) is given as

$$D^*(0)\psi = \begin{cases} -d\psi(\xi)/d\xi, & 0 < \xi \le 1, \\ \int_{-1}^{0} [d\eta_c^T(s)]\psi(-s), & \xi = 0, \end{cases} \tag{19}$$

Further, a bilinear inner product is needed to construct the center manifold reduction. For any $\psi \in C^*$ and $\phi \in C$, the bilinear inner product is defined as

$$\langle \psi,\phi \rangle = \overline{\psi}^T(0)\phi(0) - \int_{\theta=-1}^{0} \int_{\xi=0}^{\theta} \overline{\psi}^T(\xi-\theta)[d\eta(\theta)]\phi(\xi)d\xi, \tag{20}$$

such that

$$\langle \psi, D(0)\phi \rangle = \langle D^*(0)\psi,\phi \rangle.$$

Let $\Lambda = \{I\omega, -I\omega\}$ and denote Φ and Ψ^* as the bases for the generalized eigenspace P_Λ of Eq. (18) associated with Λ and its formal adjoint equation, respectively, i.e.

$$D(0)\boldsymbol{\Phi} = I\omega\Phi, \quad D^*(0)\boldsymbol{\Psi}^* = -I\omega\boldsymbol{\Psi}^*. \tag{21}$$

Solving Eq. (21), the bases obtained are

$$\begin{aligned} \boldsymbol{\Phi}(\theta) &= (1, I\omega/\tau_c, \phi_3, I\omega\phi_3/\tau_c,)^T e^{I\omega\theta}, \\ \boldsymbol{\Psi}^*(\xi) &= (\tau_c(k+a_2\varphi_4)/I\omega, 1, \tau_c(4k\varphi_4 - a_2)/I\omega, \varphi_4)^T e^{I\omega\xi}, \end{aligned} \tag{22}$$

which can be normalized by a complex scalar

$$\mathrm{B} = -\tau_c(k+a_2\overline{\varphi}_4)/I\omega + I\omega/\tau_c - \tau_c(4k\overline{\varphi}_4 - a_2)\phi_3/I\omega + I\omega\beta\phi_3\overline{\varphi}_4/\tau_c - I\omega(\alpha_{1c} + \alpha_{2c}\overline{\varphi}_4)e^{-I\omega} - I\omega(\alpha_{2c} + \alpha_{3c}\overline{\varphi}_4)\beta\phi_3 e^{-I\omega},$$

where

$$\begin{aligned} \phi_3 &= (\tau_c a_2 + (a_1 + \alpha_{2c}e^{-I\omega})I\omega)//(\omega^2/\tau_c - 4k\tau_c - I\omega(\mu_c + \alpha_{3c}e^{-I\omega})), \\ \varphi_4 &= (\tau_c\alpha_{1c}e^{I\omega} + \tau_c\mu_c - k\tau_c^2/I\omega - I\omega)/(\tau_c^2 a_2/I\omega - \tau_c a_1 - \alpha_{2c}\tau_c e^{I\omega}). \end{aligned}$$

Thus, a new basis $\boldsymbol{\Psi} = \overline{\mathrm{B}}^{-1}\boldsymbol{\Psi}^*$ is constructed with orthogonality conditions $\langle \Psi, \Phi \rangle = 1$ and $\langle \boldsymbol{\Psi}, \overline{\boldsymbol{\Phi}} \rangle = 0$ satisfied. Any element $X_t \in C$ can be decomposed by

$$X_t = \boldsymbol{\Phi}y(t) + \overline{\boldsymbol{\Phi}}\overline{y}(t) + X_t^{Q_\Lambda}, \tag{23}$$

where $y(t) \triangleq \langle \boldsymbol{\Psi}, X_t \rangle$ and Q_Λ is the complementary space of P_Λ. Substituting Eq. (23) into Eq. (18) and using the bilinear inner product defined in Eq. (20) and the orthogonality conditions, the homological equation restricted to the center manifold is written as

$$\langle \boldsymbol{\Psi}, \dot{X}_t \rangle = \langle \boldsymbol{\Psi}, (D(0)\boldsymbol{\Phi} + D_1(\overline{\nu},\overline{\alpha},\overline{\tau})\boldsymbol{\Phi}) \rangle y + \langle \boldsymbol{\Psi}, RX_t \rangle, \tag{24}$$

yielding

$$\begin{aligned} \dot{y}(t) = {} & I\omega y(t) + (\rho_1(\overline{\nu},\overline{\alpha},\overline{\tau}) + \rho_2(\overline{\nu},\overline{\alpha},\overline{\tau}))y(t) + g_{30}y^3(t) + g_{21}|y(t)|^2 y(t) \\ & + g_{12}|y(t)|^2\overline{y}(t) + g_{03}\overline{y}^3(t) + f_a\cos(\Omega_0 t) + \mathrm{O}(|y(t)|^4) \end{aligned} \tag{25}$$

where

$$\begin{aligned} \rho_1(\overline{\nu},\alpha,\overline{\tau}) = {} & -B^{-1}(I\omega(1+\overline{\varphi}_4\phi_3)\overline{\mu} + I\omega e^{-I\omega}\overline{\alpha}_1 + I\omega e^{-I\omega}(\phi_3 + \overline{\varphi}_4)\overline{\alpha}_2 \\ & + I\omega\phi_3\overline{\varphi}_4 e^{-I\omega}\overline{\alpha}_3 + (2(a_2\overline{\varphi}_4 - a_2\phi_3 + k + 4k\phi_3\overline{\varphi}_4) + I\omega/\tau_c(\alpha_{1c}e^{-I\omega} + \mu_c \\ & + a_1\overline{\varphi}_4 - a_1\phi_3 + \phi_3\alpha_{2c}e^{-I\omega} + \mu_c\overline{\varphi}_4\phi_3 + \overline{\varphi}_4\alpha_{2c}e^{-I\omega} + \phi_3\overline{\varphi}_4\alpha_{3c}e^{-I\omega}))\overline{\tau}, \end{aligned}$$

$$\rho_2(\overline{v},\overline{\alpha},\overline{\tau}) = -B^{-1}e^{-I\omega}I\omega\overline{\tau}/\tau_c(\overline{\alpha}_1+\phi_3\overline{\alpha}_2+(\overline{\alpha}_2+\phi_3\overline{\alpha}_3)\overline{\varphi}_4+(1+\overline{\varphi}_4\phi_3)e^{I\omega}\overline{\mu}),$$
$$g_{30} = -\tau B^{-1}(3f_3I\omega^3(4\tau_c^3)^{-1}(1+2\phi_3^2+2\overline{\varphi}_4\phi_3+\overline{\varphi}_4\phi_3^3)+3k_3\pi^4(1/8+\phi_3^2+\overline{\varphi}_4\phi_3+2\overline{\varphi}_4\phi_3^3)),$$
$$g_{21} = \tau B^{-1}(3f_3I\omega^3(4\tau_c^3)^{-1}(3+2\phi_3^2+4\overline{\varphi}_4\phi_3+2\overline{\varphi}_4\overline{\phi}_3+4\overline{\phi}_3\phi_3+3\overline{\varphi}_4\overline{\phi}_3\phi_3^2)$$
$$-3k_3\pi^4(3/8+\phi_3^2+2\overline{\varphi}_4\phi_3+2\overline{\phi}_3\phi_3+\overline{\varphi}_4\overline{\phi}_3+6\overline{\varphi}_4\overline{\phi}_3\phi_3^2)),$$
$$g_{12} = -\tau B^{-1}(3f_3I\omega^3(4\tau_c^3)^{-1}(3+2\overline{\phi}_3^2+4\overline{\varphi}_4\overline{\phi}_3+2\overline{\varphi}_4\phi_3+4\overline{\phi}_3\phi_3+3\overline{\varphi}_4\phi_3\overline{\phi}_3^2)$$
$$+3k_3\pi^4(3/8+\overline{\phi}_3^2+2\overline{\varphi}_4\overline{\phi}_3+\overline{\varphi}_4\phi_3+2\overline{\phi}_3\phi_3+6\overline{\varphi}_4\phi_3\overline{\phi}_3^2)),$$
$$g_{03} = \tau B^{-1}(3f_3I\omega^3(4\tau_c^3)^{-1}(1+2\overline{\phi}_3^2+2\overline{\varphi}_4\overline{\phi}_3+\overline{\varphi}_4\overline{\phi}_3^3)-3k_3\pi^4(1/8+\overline{\phi}_3^2+\overline{\varphi}_4\overline{\phi}_3+2\overline{\varphi}_4\overline{\phi}_3^3)).$$

5. Delay-induced periodic solutions and quasi-periodic solutions

As a complex ordinary differential equation, Eq. (25) exhibits the geometrical structure of the solution restricted to the center manifold of Eq. (2). At this stage, the traditional perturbation method can be adopted to analyze the approximate local solutions, which can be transformed into the original variables through Eq. (23). In the subsequent text, the analytical self-excited periodic solutions of the system without external excitations are obtained by means of Poincaré normal form in complex space. The external primary resonant responses of the string are investigated through the averaging method (c.f. [40]).

5.1. Periodic solution of non-forced system

Let f_a=0. The approximate analytical periodic solution is derived for the homological equation (25), rewritten as

$$\dot{y} = \rho(\mu)y+(g_{30}(\mu)y^3+g_{21}(\mu)|y|^2y+g_{12}(\mu)|y|^2\overline{y}+g_{03}(\mu)\overline{y}^3)+O(|y|^4), \tag{26}$$

where μ denotes the perturbation parameter i.e.$\overline{\tau}$,$\overline{\alpha}$,or $\overline{v}$, and $\rho(\mu)$=$I\omega$+$\rho_1(\mu)$+$\rho_2(\mu)$, where $\rho(\boldsymbol{0})=I\omega$, $\mathrm{Re}(\rho'(0))\neq 0$. Eq. (26) can be converted into the Poincaré normal form for all sufficiently small $|\mu|$,

$$\dot{\tilde{y}} = \rho(\mu)\tilde{y}+g_{21}(\mu)|\tilde{y}|^2\tilde{y} \tag{27}$$

with the following smooth complex coordinate transformation

$$y = \tilde{y}+h_{30}\tilde{y}^3+h_{12}\tilde{y}\overline{\tilde{y}}^2+h_{03}\overline{\tilde{y}}^3, \tag{28}$$

where

$$h_{30} = g_{30}(\mu)(2\rho(\mu))^{-1}, \quad h_{12} = g_{12}(\mu)(2\overline{\rho}(\mu))^{-1}, \quad h_{03} = -g_{03}(\mu)(\rho(\mu)-3\overline{\rho}(\mu))^{-1}$$

and the only remaining cubic term is a resonant term. Eq. (27) defines a dynamical system that is locally, topologically equivalent to the system (26) in the neighborhood of the Hopf bifurcation point, since higher-order terms in Eq. (26) do not affect the bifurcation behavior [41].

Next, the following equation is obtained with the aid of the conjugant equation of (27):

$$d(\tilde{y}\overline{\tilde{y}})/dt = 2\tilde{y}\overline{\tilde{y}}\mathrm{Re}(\rho(\mu)+g_{21}(\mu)\tilde{y}\overline{\tilde{y}}). \tag{29}$$

Therefore, $d(\tilde{y}\overline{\tilde{y}})/dt=0$ is satisfied for the steady-state periodic solution of Eq. (27), which implies

$$\tilde{y} = 0 \quad \text{or} \quad \mathrm{Re}(\rho(\mu)+g_{21}(\mu)\tilde{y}\overline{\tilde{y}}) = 0. \tag{30}$$

For periodic solutions, it follows that $\tilde{y}\overline{\tilde{y}}=\tilde{y}_s^2\neq 0$. Substituting $\mu=\mu_1\tilde{y}_s+\mu_2\tilde{y}_s^2+\cdots$into the second equation of (30) and equating coefficients of like powers of $\tilde{y}_s$, we obtain

$$\mathrm{Re}(\rho'(0))\mu_1 = 0, \quad \mathrm{Re}(g_{21}(0))+\mathrm{Re}(\rho'(0))\mu_2 = 0,$$
$$\mathrm{Re}(g'_{21}(0))\mu_1+\mathrm{Re}(\rho'(0))\mu_3+\mathrm{Re}(\rho''(0))\mu_1\mu_2 = 0, \tag{31}$$

which leads to $\mu_1=0$, $\mu_2=-\mathrm{Re}(g_{21}(0))/\mathrm{Re}(\rho'(0))$, and $\mu_3=0$.

Separating the real and imaginary parts of Eq. (27) and using the second equation of (30) again yields

$$\dot{\tilde{y}} = I\tilde{y}\mathrm{Im}(\rho(\boldsymbol{\mu})+g_{21}(\boldsymbol{\mu})\tilde{y}_s^2). \tag{32}$$

The solution to Eq. (32) can be expressed as $\tilde{y}=\tilde{y}_se^{I\tilde{\omega}(\tilde{y}_s)t}$, where $\tilde{\omega}(\tilde{y}_s)=\mathrm{Im}(\rho(\mu)+g_{21}(\mu)\tilde{y}_s^2)$. Consequently, the bifurcating periodic solution of (26) can be derived by using the inverse coordinate transformation of (28), as

$$y = \tilde{y}_se^{I\tilde{\omega}(\tilde{y}_s)t}+\tilde{y}_s^3(h_{30}e^{3I\tilde{\omega}(\tilde{y}_s)t}+h_{12}e^{-I\tilde{\omega}(\tilde{y}_s)t}+h_{03}e^{-3I\tilde{\omega}(\tilde{y}_s)t}) \tag{33}$$

and the original modal ordinates can be obtained by $X_t(0)=2\mathrm{Re}(\boldsymbol{\Phi}(0)y(t))$.

5.2. Primary resonance response of the forced system

The approximate analytical solutions of Eq. (25) can be obtained by using the averaging method. Introducing a scaling time $t\to\omega t$ and letting$y=\sqrt{\varepsilon}(y_1+Iy_2)$, $f_a=\varepsilon^{3/2}(f_{a1}+f_{a2}I)$ into the reduced form of Eq. (25) and separately equating like powers of the real and imaginary parts leads to

$$\begin{pmatrix}\dot{y}_1\\ \dot{y}_2\end{pmatrix}=\begin{bmatrix}0 & -1\\ 1 & 0\end{bmatrix}\begin{pmatrix}y_1\\ y_2\end{pmatrix}+\frac{\varepsilon}{\omega}\begin{pmatrix}k_{11}y_1+k_{12}y_2+k_{311}y_1^3+k_{312}y_1^2y_2+k_{313}y_2^2y_1+k_{314}y_2^3+f_{a1}\cos(\boldsymbol{\Omega}t)\\ k_{21}y_1+k_{22}y_2+k_{321}y_1^3+k_{322}y_1^2y_2+k_{323}y_2^2y_1+k_{324}y_2^3+f_{a2}\cos(\boldsymbol{\Omega}t)\end{pmatrix}, \tag{34}$$

where $\boldsymbol{\Omega}=\boldsymbol{\Omega}_0/\omega$, $\boldsymbol{\Omega}_0\approx\omega$, $1-\boldsymbol{\Omega}^2=\varepsilon\sigma$ and

$$\begin{aligned}
&k_{11}=k_{22}=\varepsilon^{-1}\mathrm{Re}(\rho_1+\rho_2), && k_{21}=-k_{12}=\varepsilon^{-1}\mathrm{Im}(\rho_1+\rho_2),\\
&k_{311}=\mathrm{Re}(g_{30}+g_{03}+g_{12}+g_{21}), && k_{321}=\mathrm{Im}(g_{30}+g_{03}+g_{12}+g_{21}),\\
&k_{312}=\mathrm{Im}(g_{12}-g_{21}+3g_{03}-3g_{30}), && k_{322}=\mathrm{Re}(g_{21}-g_{12}+3g_{30}-3g_{03}),\\
&k_{313}=\mathrm{Re}(g_{12}+g_{21}-3g_{30}-3g_{03}), && k_{323}=\mathrm{Im}(g_{12}+g_{21}-3g_{30}-3g_{03}),\\
&k_{314}=\mathrm{Im}(g_{12}-g_{21}+g_{30}-g_{03}), && k_{324}=\mathrm{Re}(g_{21}-g_{12}+g_{03}-g_{30}).
\end{aligned}$$

The van der Pol transformation [40]

$$\begin{pmatrix}z_1\\ z_2\end{pmatrix}=\begin{bmatrix}-\sin(\boldsymbol{\Omega}t) & \boldsymbol{\Omega}^{-1}\cos(\boldsymbol{\Omega}t)\\ \cos(\boldsymbol{\Omega}t) & \boldsymbol{\Omega}^{-1}\sin(\boldsymbol{\Omega}t)\end{bmatrix}\begin{pmatrix}y_1\\ y_2\end{pmatrix} \tag{35}$$

is adopted to rewrite Eq. (34) as follows:

$$\begin{pmatrix}\dot{z}_1\\ \dot{z}_2\end{pmatrix}=\frac{\varepsilon\sigma}{\Omega}\begin{pmatrix}\cos(\boldsymbol{\Omega}t)y_1\\ \sin(\boldsymbol{\Omega}t)y_1\end{pmatrix}+\frac{\varepsilon}{\omega}\begin{bmatrix}-\sin(\boldsymbol{\Omega}t) & \Omega^{-1}\cos(\boldsymbol{\Omega}t)\\ \cos(\boldsymbol{\Omega}t) & \Omega^{-1}\sin(\boldsymbol{\Omega}t)\end{bmatrix}\begin{pmatrix}f_1(y_1,y_2)+f_{a1}\cos(\boldsymbol{\Omega}t)\\ f_2(y_1,y_2)+f_{a2}\cos(\boldsymbol{\Omega}t)\end{pmatrix}, \tag{36}$$

which can be averaged. y_1 and y_2 are obtained by the inverse transformation of the van der Pol transformation in Eq. (35) and $f_1(y_1,y_2)$, $f_2(y_1,y_2)$ represent the non-homogeneous terms of y_1, y_2 on the right-hand side of Eq. (34). The equations of slowly varying amplitude and phase can be obtained by inserting $z_1=r(t)\sin(\phi(t))$, $z_2=r(t)\cos(\phi(t))$into Eq. (36) and averaging it over one period $T=2\pi/\boldsymbol{\Omega}$

$$\begin{aligned}
\dot{r}&=\varepsilon(P_{21}r+P_{23}r^3+P_{31}\sin(\phi)+P_{32}\cos(\phi)),\\
r\dot{\phi}&=\varepsilon(P_{11}r+P_{13}r^3+P_{31}\cos(\phi)-P_{32}\sin(\phi)),
\end{aligned} \tag{37}$$

where

$$\begin{aligned}
&P_{11}=(2\boldsymbol{\Omega}\omega)^{-1}(\sigma\omega+k_{21}-k_{12}\boldsymbol{\Omega}^2), && P_{21}=(2\omega)^{-1}(k_{11}+k_{22}),\\
&P_{31}=(2\boldsymbol{\Omega}\omega)^{-1}f_{a2}, && P_{13}=(8\boldsymbol{\Omega}\omega)^{-1}(3k_{321}+(k_{323}-k_{312})\boldsymbol{\Omega}^2-3k_{314}\boldsymbol{\Omega}^4),\\
&P_{32}=(2\omega)^{-1}f_{a1}, && P_{23}=(8\omega)^{-1}(3k_{311}+k_{322}+(k_{313}+3k_{324})\boldsymbol{\Omega}^2).
\end{aligned}$$

The equilibrium points of Eq. (37) corresponding to the phase-locked, steady-state periodic solutions of the system (34) can be solved by requesting $\dot{r}=0$, $\dot{\phi}=0$. The amplitude response equation of the periodic solution can be obtained through

$$F(r,\mu)=(P_{21}r+P_{23}r^3)^2+(P_{11}r+P_{13}r^3)^2-((2\boldsymbol{\Omega}\omega)^{-1}f_{a2})^2-((2\omega)^{-1}f_{a1})^2=0. \tag{38}$$

The phase can be obtained from Eq. (37) once the steady state amplitude is solved, and the forced response of the string restricted to the center manifold is given by

$$X_t(0)=2\varepsilon\mathrm{Re}(\boldsymbol{\Phi}(0)(r_s\cos(\boldsymbol{\Omega}t+\phi_s)+I\boldsymbol{\Omega}r_s\sin(\boldsymbol{\Omega}t+\phi_s))). \tag{39}$$

where (r_s,ϕ_s) are fixed points of Eq. (37).

The eigenvalues of the Jacobian matrix evaluated at the fixed point (r_s,ϕ_s) are solved through the characteristic equation

$$\lambda^2-P\lambda+Q=0, \tag{40}$$

where

$$P=2(P_{21}+2P_{23}r_s^2),\quad Q=P_{11}^2+P_{21}^2+4(P_{11}P_{13}+P_{21}P_{23})r_s^2+3(P_{13}^2+P_{23}^2)r_s^4.$$

The periodic solution bifurcates when there is at least one eigenvalue that is non-hyperbolic. The bifurcation point of periodic solution plays an important role in suppressing the forced response of the system. From the control point of view, the optimum of controlling parameter μ should be chosen such that $dr/d\mu=0$, $d^2r/d\mu^2>0$ (i.e. μ is the local minimum point in the(r,μ)space) for any bifurcating time delay τ_c. The most feasible controlling parameter is located in the interior of the stability region if the local optimal point cannot be found, where the amplitude of vibration is usually small.

5.3. Quasi-periodic solutions of the forced system

Design of control strategy for the axially moving strings depends on identification of quasi-periodic solution. A global analysis is needed to determine existence of the limit cycles of Eq. (37) corresponding to the quasi-periodic solutions of system (1). Rewrite Eq. (37) as

$$\begin{aligned}\dot{r} &= \varepsilon\left(P_{21}r+P_{23}r^3+\overline{p}\sin(\phi+\vartheta)\right),\\ \dot{\phi} &= \varepsilon\left(P_{11}+P_{13}r^2+r^{-1}\overline{p}\cos(\phi+\vartheta)\right),\end{aligned} \tag{41}$$

where $\overline{p}=\sqrt{P_{31}^2+P_{32}^2}$, $\cos(\vartheta)=P_{31}/\overline{p}$, $\sin(\vartheta)=P_{32}/\overline{p}$. For $\overline{p}=0$, it is found that if $P_{21}>0$ and $P_{23}<0$, a stable closed orbit exists for system (34) with the amplitude and phase

$$r(t)=r_C=\sqrt{-P_{21}P_{23}^{-1}},\quad \phi(t)=\phi_0+\varepsilon(P_{11}+P_{13}r_C^2)t. \tag{42}$$

It is supposed that the steady state amplitude $r(t)$ of the stable periodic solution is weakly perturbed for sufficiently small forcing amplitude. Thus, substituting $\tilde{r}=r-r_C$ into Eq. (41) yields

$$\begin{aligned}\dot{\tilde{r}} &= \varepsilon(-2P_{21}\tilde{r}+P_{23}\tilde{r}^3+3P_{23}\tilde{r}^2r_C+\overline{p}\sin(\phi+\vartheta)),\\ \dot{\phi} &= \varepsilon(P_{11}+P_{13}r_C^2+P_{13}(\tilde{r}^2+2\tilde{r}r_C)+(\tilde{r}+r_C)^{-1}\overline{p}\cos(\phi+\vartheta)).\end{aligned} \tag{43}$$

By assuming $\tilde{r}$ and $\overline{p}$ are small enough, the leading term of the quasi-periodic solution can be determined through

$$\dot{\tilde{r}}=\varepsilon(-2P_{21}\tilde{r}+\overline{p}\sin(\phi+\vartheta)),\quad \dot{\phi}=\varepsilon(P_{11}+P_{13}r_C^2), \tag{44}$$

Hence,

$$\begin{aligned}\tilde{r}(t)=\exp(-2P_{21}\varepsilon t)(r_0-\varepsilon\overline{p}(4\varepsilon^2P_{21}^2+\varpi^2)^{-1}(2\varepsilon P_{21}\sin(\phi_0+\vartheta)-\varpi\cos(\phi_0+\vartheta)))\\ +\varepsilon\overline{p}(4\varepsilon^2P_{21}^2+\varpi^2)^{-1}(2\varepsilon P_{21}\sin(\varpi t+\phi_0+\vartheta)-\varpi\cos(\varpi t+\phi_0+\vartheta)),\\ \phi(t)=\varpi t+\phi_0,\varpi=\varepsilon(P_{11}+P_{13}r_C^2),\end{aligned} \tag{45}$$

with initial condition $\tilde{r}(0)=r_0$, $\phi(0)=\phi_0$. In the approximate solution of (45), there exist two incommensurate frequencies, i.e. ϖ, Ω, in $X_t(0)$ and the phase angle will be increased to infinity as time increases. It is also noticed that $\phi(t)$ will oscillate with frequency ϖ, since $\tilde{r}$ and ϕ are related with each other through higher order approximation. It is observed that the amplitude of quasi-periodic solution as $t\to\infty$ becomes

$$r=r_C+\varepsilon\overline{p}(4\varepsilon^2P_{21}^2+\varpi^2)^{-1}(2\varepsilon P_{21}\sin(\varpi t+\phi_0+\vartheta)-\cos(\varpi t+\phi_0+\vartheta)\varpi). \tag{46}$$

Alternatively, other quasi-periodic solutions of system (34) can be revealed by using the Poincaré–Bendixson theorem. A trapping region, denoted by $(r_C^\circ,\widehat{r}_C)$, that contains an isolated closed orbit can be constructed if there exist two concentric circles with radii r_C° and $\widehat{r}_C$ such that $\dot{r}>0$ on the inner circle $r=r_C^\circ$ and $\dot{r}<0$ on the outer circle $r=\widehat{r}_C$. Note that $\dot{r}>0$ holds for any sufficiently small circle enclosing an unstable focus or node of system (41). In the following, the outer circle to confine all trajectory flows will be found.

The non-existence condition of closed orbits of Eq. (34) is firstly considered by an energy approach [25–27]. Let $A=r^2$, Eq. (41) can be rewritten as

$$\begin{aligned}\dot{A} &= 2\varepsilon(P_{21}A+P_{23}A^2+\sqrt{A}\overline{p}\sin(\phi+\vartheta)),\\ \dot{\phi} &= \varepsilon(P_{11}+P_{13}A+(\sqrt{A})^{-1}\overline{p}\cos(\phi+\vartheta)).\end{aligned} \tag{47}$$

Introducing an energy-like function

$$E(A,\phi)=\varepsilon(P_{11}A+1/2P_{13}A^2+2\sqrt{A}\overline{p}\cos(\phi+\vartheta)). \tag{48}$$

The derivative of the E function can be obtain using Eq. (47),

$$\dot{E}=2\varepsilon A(P_{21}+P_{23}A)\dot{\phi}. \tag{49}$$

Hence, the increment of the E function evaluated on a closed orbit is determined

$$\Delta E=\int_0^T\dot{E}dt=\int_0^{2\pi}2\varepsilon A(P_{21}+P_{23}A)d\phi. \tag{50}$$

It can be demonstrated that for Eq. (50), if $P_{21}P_{23}>0$ for $r>r_C$ or $P_{21}P_{23}<0$ for $r<r_C$ in the region defined, there is no limit cycle corresponding to the bounded-phased quasi-periodic solution of Eq. (34), since $\Delta E\neq 0$. The necessary condition for existence of the modulated quasi-periodic solutions is $P_{21}P_{23}<0$ and the flow must cross the boundary of the trapping region outwardly. Satisfaction of these conditions gives the upper boundary of the trapping region from the first equation of (47)

$$P_{21}A_R+P_{23}A_R^2+\sqrt{A_R}\overline{p}<0 \tag{51}$$

on condition that $\sin(\phi+\vartheta)\le 1$. The trapping region $(r_C^\circ,\sqrt{A_R})$ can be constructed if condition $\sqrt{A_R}>r_C^\circ$ is satisfied.

In the next section, the two different quasi-periodic solutions are illustrated with varying time delays.

6. Numerical illustrations

The explicit dynamics of both periodic and quasi-periodic solutions derived above are illustrated with examples focusing on the effect of time delay. The numerical integration is performed to examine the validity and accuracy of the analytical explicit solutions. The BS (2, 3) Runge–Kutta method for solving delayed differential equations (DDEs) is adopted to obtain numerical results [36].

An axially moving string without external loadings is selected as the first example with parameters: $\alpha_c=-2,\overline{\alpha}=0,\tau_c=0.16465,\nu_c=0.1,\overline{\nu}=0$ and k_3=5. As shown in Fig. 2 the critical point is located on curve $\tau_{c0,1}$ through which the second mode of system (1) becomes unstable with increasing time delay such that the supercritical Hopf bifurcation occurs. The second mode dominates the corresponding bifurcating periodic solutions since the component of the first mode in the response is extinguished for a sufficiently long time. The approximate solution of the second mode and the numerical simulation with several perturbations of time delay are shown in Fig. 4, where the approximate solutions are obtained

$$q_2(t)=0.2334\sqrt{\overline{\tau}}\sin(\tilde{\omega}\tau^{-1}t)-0.2684\sqrt{\overline{\tau}}\cos(\tilde{\omega}\tau^{-1}t)+O(\sqrt{\overline{\tau}}^3),$$

$$\dot{q}_2(t)=-2.5501\sqrt{\overline{\tau}}\sin(\tilde{\omega}\tau^{-1}t)-2.2176\sqrt{\overline{\tau}}\cos(\tilde{\omega}\tau^{-1}t)+O(\sqrt{\overline{\tau}}^3),$$

where the frequency is $\tilde{\omega}=1.5644+13.1008\overline{\tau}+O(\overline{\tau}^2)$.Fig. 4 shows that the analytical solutions are capable of predicting bifurcation of the periodic solutions when the time delay is nearly critical. There is a noticeable diversity when the perturbation of time delay is large since the center manifold is essentially accurate only for reduction of local dynamics.

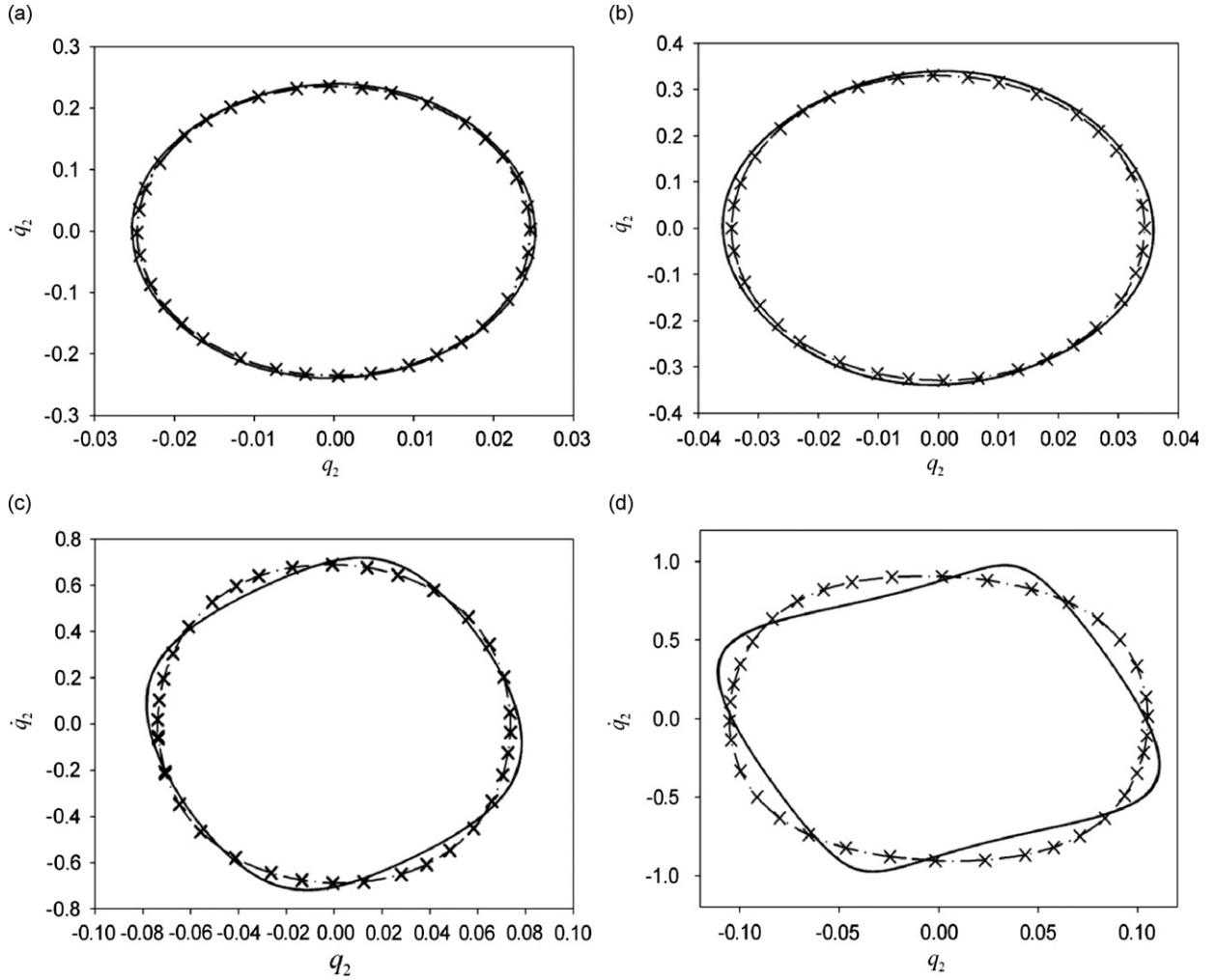

Fig. 4. A comparison between the approximate solutions and the numerical solutions of the second mode in phase space for different time delays: (a) $\overline{\tau}=0.005$, (b) $\overline{\tau}=0.01$, (c) $\overline{\tau}=0.05$, and (d) $\overline{\tau}=0.1$, where the approximate solutions and the numerical solutions are represented by the solid lines and the dash-dotted lines with crossing symbols, respectively.

Nevertheless, the analytical expression can be used as initial condition for an improved numerical solution. The analytical solutions and numerical results of forced axially moving strings differ in a similar manner when the frequency is closed to the critical frequency in the sense that the frequency of the periodic solutions of the forced system is phase-modulated.

As for the forced systems, we focused on the bifurcation of periodic solutions and analyzed the effect of time delay and external excitations on local dynamics of the system. Two systems denoted by **I** and **II** are analyzed. Parameters τ_c=0.2, α_c= −1.1349, β_c=7.7881and $\overline{\alpha}=-0.01$ are assigned to system **I** and τ_c=2.18, α_c= −0.21986, $\beta_c=6.4425$,$\overline{\alpha}=0$ to system **II** with $\overline{\mu}=0,\nu=0.1,\varepsilon^{-3/2}f_a$=0.5 throughout. It can be seen from Fig. 2 that the selected Hopf points are located at $\tau_{c0,1}$ and $\tau_{c2,1}$, at the right boundary of the stable regions **I** and **II**, respectively. For system **I**, the averaged equations of the reduced equation on the center manifold which are obtained by substituting the numerical values of the corresponding coefficients in Eq. (37) are found to be

$$\begin{aligned}\dot{r} &= \varepsilon((0.000747+1.739179\overline{\tau})r-(96.566071\boldsymbol{\Omega}^2+482.830353\overline{\tau}\boldsymbol{\Omega}^2+96.913411+484.567055\overline{\tau})r^3\\ &\quad+0.000011(0.2+\overline{\tau})^2\boldsymbol{\Omega}^{-2}\sin(\phi)+0.000002(0.2+\overline{\tau})^2\cos(\phi)),\\ r\dot{\phi} &= \varepsilon((2.174851\overline{\tau}(1+\boldsymbol{\Omega}^2)+0.500982-0.499018\boldsymbol{\Omega}^2)\boldsymbol{\Omega}^{-1}r+(133.118652\boldsymbol{\Omega}^{-1}+665.593261\overline{\tau}\boldsymbol{\Omega}^{-1}\\ &\quad+168.58179\boldsymbol{\Omega}+842.908951\overline{\tau}\boldsymbol{\Omega}+37.286419\boldsymbol{\Omega}^3+186.432093\overline{\tau}\boldsymbol{\Omega}^3)r^3\\ &\quad+0.000011(0.2+\overline{\tau})^2\boldsymbol{\Omega}^{-2}\cos(\phi)-0.000002(0.2+\overline{\tau})^2\sin(\phi)).\end{aligned} \tag{52}$$

The phase-locked periodic solutions, i.e. the fixed points of Eq. (13), are obtained numerically through solving Eq. (52) by requiring $\dot{r}=\dot{\phi}=0$. The amplitudes for systems I and II are shown in Fig. 5(a) with $\overline{\tau}=0.01$, where the solid and dashed lines represent stable and unstable motions, respectively. The curves of the amplitude are also marked by letters F and N, which stand for fixed points of focus and node, respectively. The stable periodic solutions of primary resonance only exist

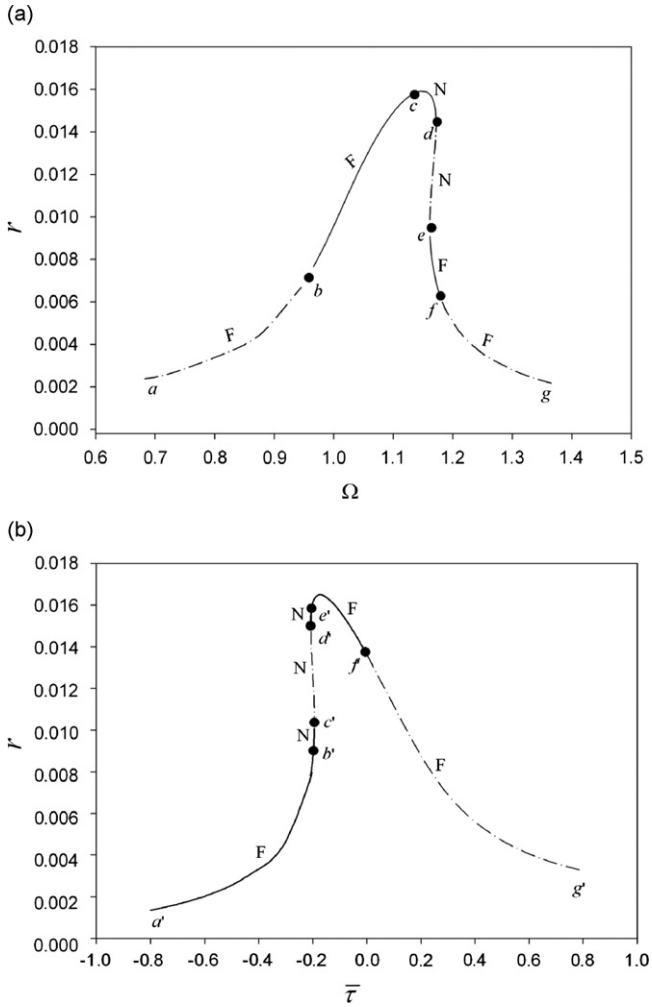

Fig. 5. The external excitation–response curves of the reduced equation for system **I** and **II**: (a) amplitude response curve for system **I** with $\overline{\tau}=0.01$ and (b) the influence of the time delay on the amplitude with the fixed excitation parameter σ= −0.050625 for system **II**, where stable equilibrium and unstable equilibrium are denoted by solid line and dashed line, respectively, and F represents focus, N for node.

for external frequency $\Omega \in (0.94925, 1.17196)$, shown as segments ($b$, c), (e, f) and (c, d) in Fig. 5(a). Other segments on the amplitude curve are unstable foci (a, b) and (f, g), and unstable node (d, e). For system **II**, the $r-\overline{\tau}$ curve in Fig. 5(b) shows the amplitude of a typical soft-spring system. The stability of the periodic solutions is different from that of system **I**. The stable foci are shown as segments (a', b') and (e', f'), and the stable nodes are shown as (b', c') and (d', e'). The unstable node is shown as segment (c', d') and unstable focus is shown as segment (f', g').

To demonstrate the influences of time delay on bifurcation of periodic solutions in the case of primary resonance, the three dimensional space $(\overline{\tau}, r, \boldsymbol{\Omega})$ is shown in Fig. 6(a) for system **I** with f_a=0.5, and $(\overline{\tau}, r, f_a)$ is shown in Fig. 6(b) for system **II** with $\sigma = -0.050625$. The solid lines are zeroes of determinant of the characteristic polynomial, i.e. $\Delta = \sqrt{P^2 - 4Q}$, in Eq. (40).The dotted-dashed lines are points of P=0, and dashed lines are those of Q=0, respectively. The stability boundaries are crucial for determining the feasible interval of controlling time delay for given forcing frequencies or amplitudes, since conditions for minimizing r: $dr/d\overline{\tau} = 0, \quad d^2r/d\overline{\tau}^2 > 0$ are not satisfied in this case. Based on Eq. (40), the stability can be changed in two ways. One is that Q=0, $P < 0$ corresponding to the boundary of saddle to stable node marked by downward triangles in Fig. 6. The other is P=0,$Q > 0$ representing the separatrix of stable focus and unstable focus marked by upward triangles. For system **I**, the interior of the curved surface S as shown in Fig. 6(a) formed by those two boundaries is the stable region. By contrast, there exist two similar curved surfaces $\tilde{S}_1$ and $\tilde{S}_2$ for system **II**, where the amplitude of periodic solutions in $\tilde{S}_1$ is smaller than that of $\tilde{S}_2$. For clarity, the bifurcation curves are projected to parametric spaces $(\overline{\tau}, r)$ and the

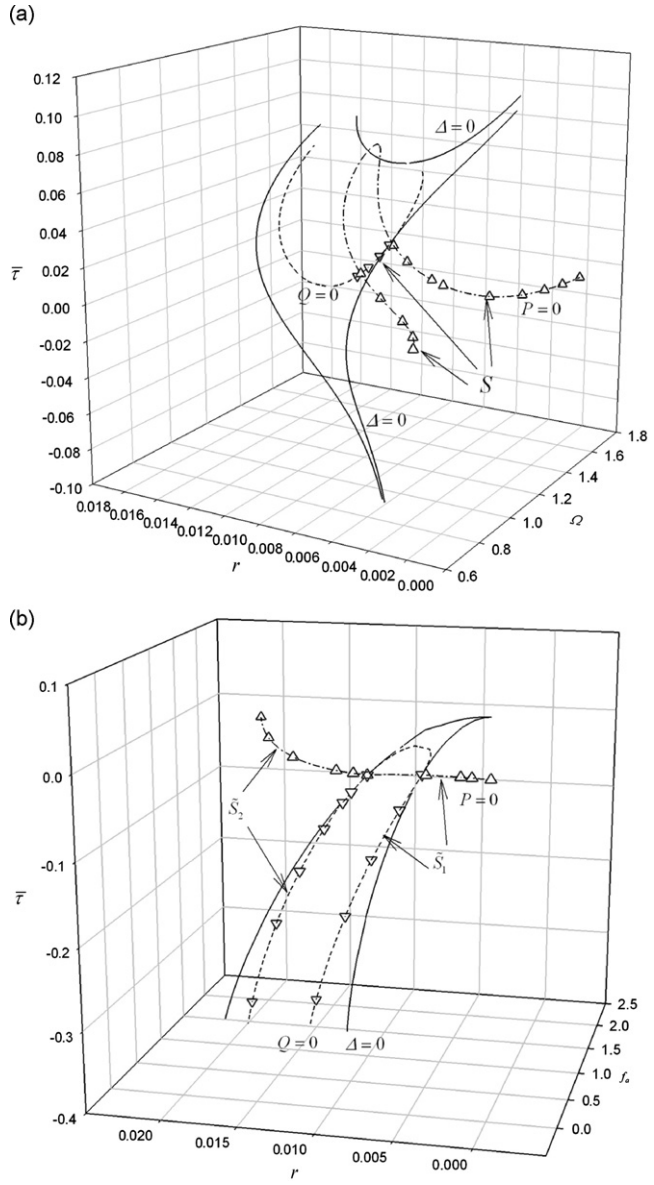

Fig. 6. The bifurcation curves and the stable regions of periodic solutions for (a) system **I** with f_a=0.5 and (b) system **II** with $\boldsymbol{\sigma} = -0.050625$.

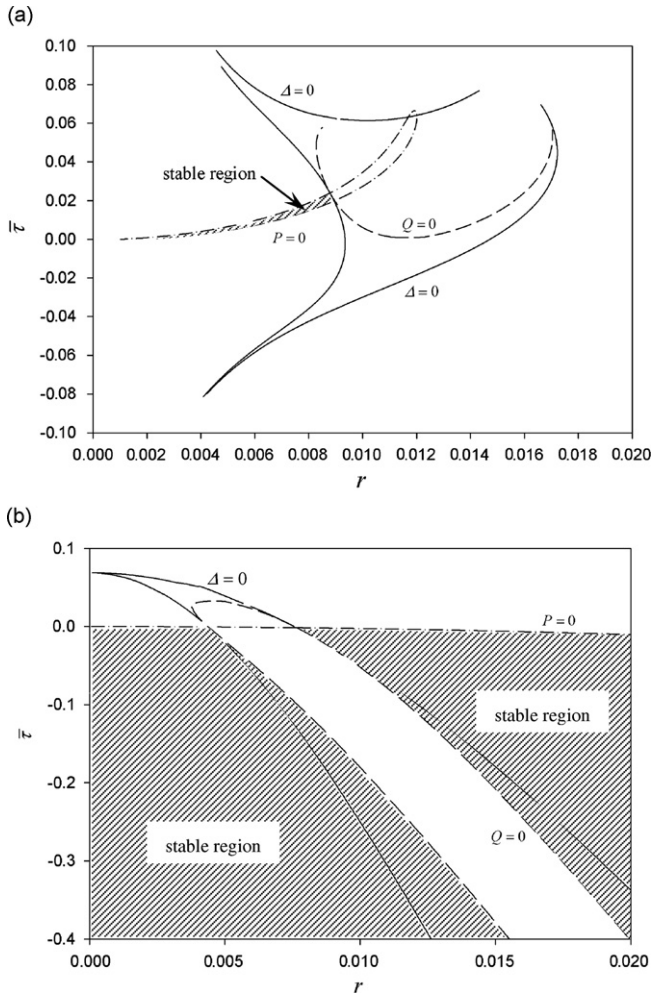

Fig. 7. The stable regions of periodic solutions in two dimensional spaces $(\overline{\tau},r)$for (a) system **I** with f_a=0.5 and (b) system **II** with $\sigma=-0.050625$.

stable regions are denoted by shaded areas for system **I** with f_a=0.5 in Fig. 7(a)(Ω is not shown) and for system **II** with $\sigma=-0.050625$ in Fig. 7(b) (f_a is not shown).

Next, the quasi-periodic solutions in the unstable regions of periodic solutions of the system **I** are discussed. For system **I** with $\overline{\tau}=0.01$, it is obtained that P_{21}=0.01814 > 0 and $P_{23}=-(101.3944\Omega^2+101.7591)<0$. The two kinds of quasi-periodic solutions analyzed in Section 5.3 are found by numerically solving the averaged equation of the reduced system, as shown in Fig. 8(a, b). Fig. 8(a) shows the time trajectory of the phase angle and the phase portrait of the local coordinate on the center manifold of the quasi-periodic solutions with infinite phase when Ω=0.9. For Ω=1.2, the equilibrium (r_C=0.008557) of system **I** is an unstable focus and we expect that there exists a unique one-period quasi-periodic solution. The corresponding limit cycle is predicted in the annals (0, 0.01047) of coordinates z_1 and z_2. It is shown in Fig. 8(b) that the numerical result of the limit cycle is restricted in (0.001218, 0.009551) in magnitude, which is in good agreement with the analytical prediction. To identify the predicted quasi-periodic solutions, the Poincaré mapping method is used through defining a Poincaré plane as $\{(q_1(t),\dot{q}_1(t))|q_2(t)>0,\dot{q}_2(t)=0\}$. The initial conditions $(q_1,\dot{q}_1,q_2,\dot{q}_2)=(0.01,0,-0.05,0)$ are used along with trivial histories of time delay. In Fig. 9, the Poincaré map for the original modal ordinates corresponding to quasi-periodic solutions of system **I** is demonstrated, where Ω=0.9 in Fig. 9(a) and Ω=1.2 in Fig. 9(b).

7. Discussions and conclusions

In this paper, the local dynamics near the Hopf bifurcation points for an axially moving string under wind excitations with a direct linear time-delayed velocity feedback controller is analytically developed through the center manifold reduction. For the subcritical system of the string, the stability of static configuration is analyzed and multiple stable

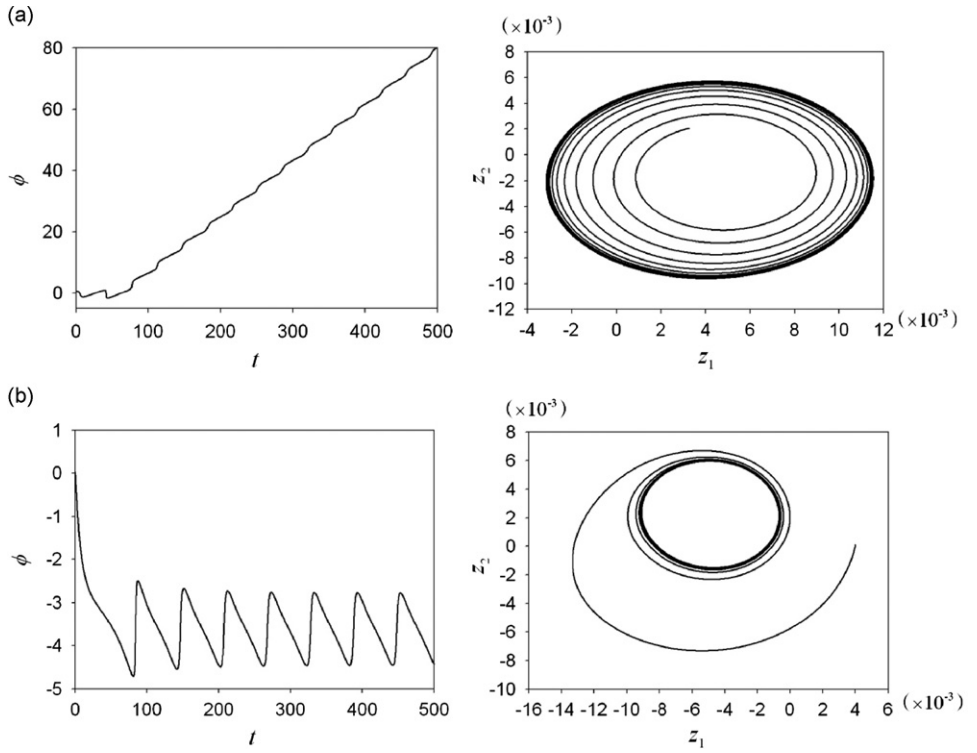

Fig. 8. Limit cycles of the reduced equation of system **I** for (a) Ω=0.9 and (b) Ω=1.2.

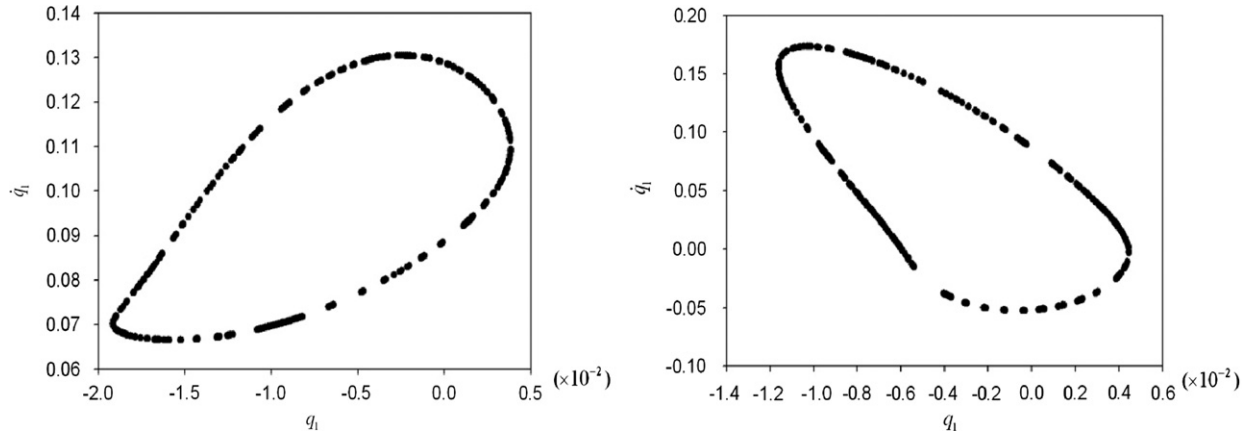

Fig. 9. Poincaré maps of the quasi-periodic solutions for system **I** (a) Ω=0.9 and (b) Ω=1.2, where the Poincaré plane is taken from $(q_1,\dot{q}_1)$ with $q_2>0,\dot{q}_2=0$.

regions are found in the controlling parameter spaces (α,τ), in which the responses of the self-excited system are suppressed. It is observed that the stability of the equilibrium of the controlled system without time delay is not affected by small time delays. In addition, the equilibrium loses its stability through Hopf bifurcation. The reduced system's dynamics on the center manifold is derived through the center manifold reduction. After the Hopf bifurcation the approximate analytical steady-state periodic solutions of the controlled system are obtained in the neighborhood of the Hopf bifurcation points with no external excitations and with primary resonance excitation through the perturbation method. The bifurcation diagrams of the periodic solutions show that time delay has a significant effect on the dynamics of the system. Based on numerical results, the local perturbation time delay is capable of suppressing vibration responses of the string. Quasi-periodic motions can be observed and are expected when the periodic solutions become unstable. One has an infinite phase and the other is one-periodic quasi-periodic solution with a periodic time-varying phase. The numerical results demonstrated the validity of the analytical prediction.

It is known that there are at most two periodic solutions for self-excited system if the first two coupling modes are considered in the uncontrolled system without external excitations. Each of the solutions is related to either the first or the second mode separately, acting like two single degree-of-freedom oscillators. Presence of the time delay leads to the change in the total number of Hopf bifurcation. It is an interesting question that whether or not the two additive Hopf bifurcations have an effect on the number of limit cycles, which can be considered as the extension of the second part of Hilbert's sixteenth problem. The answer to this question may involve the center manifold reduction with unstable manifolds. Further discussion is expected on global optimal control of the string vibration. In spite of these open problems yet to be solved, the techniques developed and applied in the present paper have obvious applications in practice.

Acknowledgement

The authors thank the Natural Science Foundation of China (Projects 10721062 and 10472021) and the National 863 (Project 2007AA04Z405) for funding this research. They are also indebted to Professor C. E. Falbo for his notes on Functional Differential Equations and to the anonymous reviewer for his or her helpful comments.

References

[1] C.D. Mote Jr., Dynamic stability of axially moving materials, *The Shock and Vibration Digest* 4 (1972) 2–11.
[2] J.A Wickert, C.D. Mote Jr., Current research on the vibration and stability of axially-moving materials, *The Shock and Vibration Digest* 20 (5) (1988) 3–13.
[3] L.Q. Chen, Analysis and control of transverse vibrations of axially moving strings, *Applied Mechanics Reviews* 58 (2005) 91–116.
[4] L.Q. Chen, W. Zhang, J.W. Zu, Nonlinear dynamics for transverse motion of axially moving strings, *Chaos, Solitons and Fractals* 40 (2009) 78–90.
[5] P.C. Hughes, R.E. Skelton, Controllability and observability of linear matrix-second-order systems, *Journal of Applied Mechanics* 47 (2) (1980) 415–420.
[6] B. Yang, C.D. Mote Jr., Controllability and observability of distributed gyroscopic systems, *Journal of Dynamic Systems, Measurement, and Control* 113 (1) (1991) 11–17.
[7] B. Yang, C.D. Mote Jr., Frequency-domain vibration control of distributed gyroscopic systems, *Journal of Dynamic Systems, Measurement, and Control* 113 (1) (1991) 18–25.
[8] B Yang, C.D. Mote Jr., Active vibration control of the axially moving string in the S domain, *Journal of Applied Mechanics* 58 (1) (1991) 189–196.
[9] B Yang, Noncollocated control of a damped string using time delay, *Journal of Dynamic Systems, Measurement, and Control* 114 (4) (1991) 736–740.
[10] C.H. Chung, C.A. Tan, Active vibration control of the axially moving string by wave cancellation, *Journal of Vibration and Acoustic* 117 (1) (1995) 49–55.
[11] C.A. Tan, S. Ying, Active wave control of the axially moving string: theory and experiment, *Journal of Sound and Vibration* 236 (5) (2000) 861–880.
[12] W. Zhang, L.Q. Chen, Vibration control of an axially moving string system: wave cancellation method, *Applied Mathematics and Computation* 175 (2006) 851–863.
[13] R.F. Fung, C.C. Tseng, Boundary control of an axially moving string via Lyapunov method, *Journal of Dynamic Systems, Measurement, and Control* 121 (1999) 105–110.
[14] T.C. Li, Z.C. Hou, J.F. Li, Stabilization analysis of a generalized nonlinear axially moving string by boundary velocity feedback, *Automatica* 44 (2008) 498–503.
[15] R.F. Fung, C.C. Liao, Application of variable structure control in the nonlinear string system, *International Journal of Mechanical and Sciences* 37 (9) (1995) 985–993.
[16] R.F. Fung, J.S. Huang, Y.C. Wang, R.T. Yang, Vibration reduction of the nonlinearly traveling string by a modified variable structure control with proportional and integral compensations, *International Journal of Mechanical Sciences* 40 (6) (1998) 493–506.
[17] D.V. Ramana Reddy, A. Sen, G.L. Johnston, Dynamics of a limit cycle oscillator under time delayed linear and nonlinear feedbacks, *Physica D* 144 (2000) 335–357.
[18] S.A. Campbell, J. Bélair, T. Ohira, J. Milton, Complex dynamics and multistability in a damped harmonic oscillator with delayed negative feedback, *Chaos* 5 (4) (1995) 640–645.
[19] J. Xu, K.W. Chung, Effects of time delayed position feedback on a van der Pol-Duffing oscillator, *Physica D* 180 (2003) 17–39.
[20] J. Xu, K.W. Chung, C.L. Chan, An efficient method for studying weak resonant double Hopf bifurcation in nonlinear systems with delayed feedbacks, *SIAM Journal on Applied Dynamical Systems* 6 (1) (2007) 29–60.
[21] J. Xu, P. Yu, Delay-induced bifurcations in a nonautonomous system with delayed velocity feedbacks, *International Journal of Bifurcation and Chaos* 14 (8) (2004) 2777–2798.
[22] Z.H. Wang, H.Y. Hu, An energy analysis of nonlinear oscillators with time-delayed coupling, *International Journal of Bifurcation and Chaos* 16 (8) (2006) 2275–2292.
[23] J.C. Ji, N. Zhang, Additive resonances of a controlled van der Pol-Duffing oscillator, *Journal of Sound and Vibration* 315 (1–2) (2008) 22–33.
[24] J.C. Ji, C.H. Hansen, Stability and dynamics of a controlled van der Pol-Duffing oscillator, *Chaos, Solitons and Fractals* 28 (2006) 555–570.
[25] A. Maccari, Modulated motion and infinite-periodic homoclinic bifurcation for parametrically excited Liénard systems, *International Journal of Non-Linear Mechanics* 35 (2000) 239–262.
[26] A. Maccari, Vibration control for parametrically excited Liénard systems, *International Journal of Non-Linear Mechanics* 41 (2006) 146–155.
[27] A. Maccari, Vibration amplitude control for a van der Pol-Duffing oscillator with time delay, *Journal of Sound and Vibration* 317 (2008) 20–29.
[28] B. Yang, C.D. Mote Jr., On time delay in noncolocated control of flexible mechanical systems, *Journal of Dynamic Systems, Measurement, and Control* 114 (3) (1992) 409–415.
[29] A.C.J. Luo, C.D. Mote Jr., Equilibrium solutions and existence for traveling, arbitrarily sagged, elastic cables, *Journal of Applied Mechanics* 67 (1) (2000) 148–154.
[30] Y.F. Wang, L.F. Lu, L.H. Huang, Analysis and design optimization of axially moving structures with stability constraint under wind excitations, *Advances in Structural Engineering* 10 (6) (2007) 655–661.
[31] L.F. Lu, Y.F. Wang, Y.X. Liu, On self-excited vibration analysis for axially moving string with transverse wind excitations, *Engineering Mechanics* 25 (2) (2008) 40–45 in Chinese.
[32] J.K. Hale, in: *Theory of Functional Differential Equations*, Springer-Verlag, New York, 1977.
[33] Y.X. Qin, Y.Q. Liu, L. Wang, Z.M. Zheng, *Stability of Motion for Dynamic Systems with Time Delay*, *Bei Jing*, Science Press, 1989 in Chinese.
[34] J. Bélair, S.A. Campbell, Stability and bifurcations of equilibria in a multiple-delayed differential equation, *SIAM Journal on Applied Mathematics* 54 (5) (1994) 1402–1424.
[35] T. Estermann, in: *Complex Numbers and Functions*, The Athlone Press, University of London, London, 1962.

[36] L.F. Shampine, S. Thompson, Solving DDEs in MATLAB, *Applied Numerical Mathematics* 37 (2001) 441–458.
[37] B.D. Hassard, N.D. Kazarinoff, Y.H. Wan, in: *Theory and Applications of Hopf Bifurcation*, Cambridge University Press, Cambridge, 1981.
[38] N. Chafee, A bifurcation problem for a functional differential equation of finitely retarded type, *Journal of Mathematical Analysis and Applications* 35 (1971) 312–348.
[39] D.G. Hartig, The Riesz representation theorem revisited, *The American Mathematical Monthly* 90 (4) (1983) 277–280.
[40] J. Guckenheimer, P. Holmes, in: *Nonlinear Oscillations, Dynamical Systems, and Bifurcations of Vector Fields*, Springer-Verlag, New York, 1983.
[41] Y.A. Kuznetsov, in: *Elements of Applied Bifurcation Theory*, Springer-Verlag, New York, 1995.